International Journal of Fracture **99:** 81–95, 1999.

Edge-cracks in single crystals under monotonic and cyclic loads

JOHN W. HUTCHINSON[1] and VIGGO TVERGAARD[2]
[1]*Division of Engineering and Applied Sciences, Harvard University, Cambridge, MA 02138, U.S.A.*
[2]*Department of Solid Mechanics, Technical University of Denmark, DK-2800 Lyngby, Denmark*

Received 5 June 1997; accepted in revised form 27 January 1998

Abstract. Basic solutions are obtained for edge-cracks lying along the primary slip plane in a single crystal. The study is motivated by Stage I fatigue crack growth wherein crack orientation is controlled by the slip direction and continued growth is dependent on the crack overcoming barriers to slip. Plasticity is assumed to occur as slip along planes inclined at 45° to the surface. Problems where slip is limited to persistent slip bands are considered side-by-side with the problem where slip is not confined. Results for both monotonic and cyclic loadings are presented, with emphasis on the crack tip opening and sliding displacements. Both small and large scale yielding are considered. Preliminary results are given for interaction with barriers to slip, such as a grain boundary.

Key words: Edge-cracks, fatigue, single crystals, large scale yielding.

1. Introduction

Under cyclic loading, single crystals of certain metals are observed to develop small fatigue cracks parallel to persistent slip bands (PSBs), usually along one of the boundaries between the band and the surrounding crystal (Ma and Laird, 1989). Cracks are nucleated with densities comparable to the density of the PSBs (e.g., as many as hundreds per centimeter (Ma and Laird, 1989)). Nucleation of these cracks is thought to be connected with the build-up of local stresses and extruded material where the PSB intersects the surface of the crystal (see Repetto and Ortiz (1997) for recent developments and relevant references). Under continuing cyclic loading, a few of the cracks grow large enough to become full fledged fatigue cracks, but the vast majority appear to arrest and remain innocuous. In the observations of the copper single crystal by Ma and Laird, the width of a PSB is on the order of one micron, while the typical arrested crack extends several microns or more into the crystal from the surface. Those that become full fledged fatigue cracks continue growing beyond this length. The early stages of cracking for crystals and for structural polycrystalline metal alloys which do not form persistent slip bands is thought to be qualitatively similar to that just described. Small cracks undergo Stage I growth along favorably oriented primary slip planes at approximately 45° to the surface and either arrest at some barrier or succeed in transitioning to Stage II and become a small mode I crack (Miller, 1993; McDowell, 1996).

The aim of the present study is to provide some basic results for 45° edge-cracks that will be useful in formulating a mechanics of Stage I fatigue crack growth. Three situations are depicted in Figure 1: a crack lying along the direction of the slip plane where slip is not confined in (a), and a crack lying along one side or the other of a PSB in (b) and (c). The slip planes and the band are oriented at 45° measured from the surface of the crystal, corresponding to the plane of maximum shear stress magnitude for inplane stressing parallel to the edge. The crack has length a. The band width is w for the PSB models. Two-dimensional, plane strain

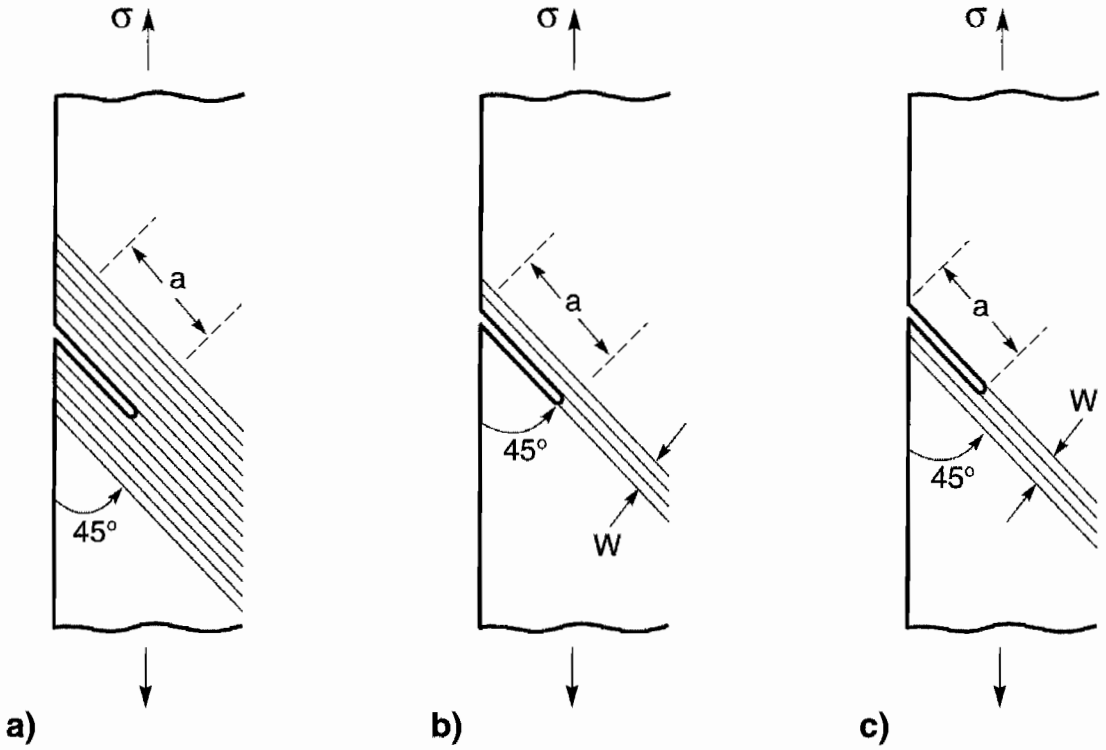

Figure 1. A 45° edge-crack aligned with the slip plane in a single crystal and subject to inplane tensile stress σ. (a) Unconfined slip. (b) and (c) Slip confined to a band of width w above or below the crack.

conditions are assumed with a remote tensile stress σ acting parallel to the free surface of the crystal. The elastic properties of the crystal are taken to be isotropic with Young's modulus E and Poisson's ratio ν. The model will be investigated under monotonically increasing σ and under tensile loadings where σ is cycled between minimum and maximum values. In the last part of the paper, barriers to slip will be modeled to assess their effect on deformation at the crack tip.

When plasticity is completely suppressed, the elastic stress intensity factors K_I and K_{II} for an inclined edge-crack have been given by Isida (1979). For an edge-crack of length a at 45° to the free edge of a semi-infinite plane, slanted downward as in Figure 1,

$$K_I = 0.705\sigma\sqrt{\pi a} \quad \text{and} \quad K_{II} = -0.364\sigma\sqrt{\pi a}. \tag{1.1}$$

Thus the mode ratio, $K_{II}/K_I \cong -1/2$, pertains approximately for this crack when the stress is such that small scale yielding applies.

Only slip on the primary slip system is allowed. The mutually orthogonal slip direction and slip plane normal are designated by $(\mathbf{t}, \mathbf{n})$. The slip system is modeled as elastic-perfectly plastic with slip activated by a critical resolved shear stress τ_Y. For the PSB problems, slip is confined to a band, whereas in the other case slip is free to occur where the resolved shear stress exceeds τ_Y. The nonzero plastic strain rate component is

$$\dot{\varepsilon}^p_{nt} = \dot{\varepsilon}^p_{tn} = \tfrac{1}{2}\dot{\gamma}, \tag{1.2}$$

where the slip rate $\dot{\gamma}$ must be consistent with

$$\dot{\gamma} \geqslant 0 \quad \text{for} \quad \sigma_{nt} = \tau_Y, \qquad \dot{\gamma} \leqslant 0 \quad \text{for} \quad \sigma_{nt} = -\tau_Y, \quad \text{and}$$

$$\dot{\gamma} = 0 \quad \text{for} \quad |\sigma_{nt}| < \tau_Y, \tag{1.3}$$

where $\sigma_{nt} = \sigma_{ij} n_i t_j$.

The components of the crack tip displacement are denoted by (δ_t, δ_n), corresponding to tangential sliding and a normal opening components. Amplitudes of the changes in these components in steady cycling between $\sigma_{\min}$ and $\sigma_{\max}$ are denoted by $(\Delta\delta_t, \Delta\delta_n)$. The range of the cyclic applied stress is assumed to be such that crack closure does not occur. Crack tip displacements are featured in this study. At the level of the continuum modeling pursued here, these measures of crack tip deformation are likely to the most useful for correlating fatigue crack growth. The magnitudes of the two tip components change relative to one another as the scale of yielding changes and as the tip encounters obstacles. It remains an important open task to identify crack growth criteria under mixed mode conditions.

2. Numerical models

Two types of numerical models have been employed to analyze the various problems posed in this paper. Primary emphasis has been put on obtaining relationships between the components of crack tip displacement and the loading history. A finite element model with a grid specially designed for single slip plasticity has served as the primary numerical method. Features of the solution brought out by the finite element results reveal that in some instances an extended Dugdale (1960) – Barenblatt (1959a, 1959b, 1962) model can provide an effective approximation. When applicable, the double slip zone model has certain numerical advantages over the finite element model.

2.1. Finite element model

In the elastic-plastic material with single slip specified by (1.3), the total strain rate is taken to be the sum of an elastic part and a plastic part, $\dot{\varepsilon}_{ij} = \dot{\varepsilon}^e_{ij} + \dot{\varepsilon}^p_{ij}$. The elastic part satisfies Hooke's law, $\dot{\sigma} = \ell_{ijkl}\dot{\varepsilon}^e_{kl}$, where ℓ_{ijkl} are the elastic instantaneous moduli. The plastic part satisfies $\dot{\varepsilon}^p_{ij} = \dot{\gamma}\alpha_{ij}$ (see also (1.2)), where $\alpha_{ij} = \frac{1}{2}(s_i n_j + s_j n_i)$ in terms of the slip direction s_i and the slip plane normal n_i. Then, the elastic-plastic incremental constitutive relation is of the form

$$\dot{\sigma}_{ij} = L_{ijkl}\dot{\varepsilon}_{kl}, \qquad L_{ijkl} = \ell_{ijkl} - \mu M_{ij} M_{kl} \tag{2.1}$$

where $\mu = 1/(\alpha_{mn} M_{mn})$ for plastic yielding and $\mu = 0$ for elastic unloading. Furthermore, $M_{ij} = E\alpha_{ij}/(1+\nu)$, in terms of Young's modulus E and Poisson's ratio ν.

The requirement of equilibrium is specified in terms of the incremental principle of virtual work. Approximate solutions are obtained by the finite element method, using the incremental constitutive relation (2.1) in the principle of virtual work. The element approximation of the displacement components is based on eight-noded isoparametric elements, and the integrations within each element, needed to compute the incremental stiffness matrix, are carried out using 2×2-point Gaussian quadrature.

Two types of boundary conditions are used in the present analyses. When conditions of small scale yielding are considered, a circular region is analyzed with displacement boundary

conditions prescribed on the outer edge in agreement with the mixed-mode singular elastic crack tip fields. When an edge-crack in a specimen under uniaxial plane strain tension is considered, a rectangular region is analyzed with uniform axial displacements and zero shear stress prescribed on the ends. The lateral sides are traction-free. The traction-free edge-crack inclined to the tensile direction is located at the middle of one of these traction-free sides.

The grid near the crack tip is particularly chosen to represent the characteristic near-tip strain fields. There is a tendency for plastic slip to concentrate in a narrow band along the extended crack plane ahead of the crack tip. In case of a finite size specimen, this narrow band eventually develops into a slip band which extends across the specimen. Some of the present computations have been continued until this stage, where the overall tensile load approaches the limit load for the cracked crystal. With the deformation mechanism allowing for single slip in directions parallel to the crack plane there is also a tendency for concentrated plastic shearing to develop from the crack tip in a direction perpendicular to the crack plane (and thus perpendicular to the slip planes). As discussed by Saeedvafa and Rice (1992), the slip system (1.2) allows concentrated shearing along planes perpendicular to the slip plane (interpretable in dislocation terms as a kink band), as well as in directions parallel to the slip plane. To represent localized yielding in these two characteristic directions, the near tip mesh has been specially designed with narrow element bands of constant width along these directions, as seen in Figure2. Comparison with analyses for a standard mesh at a crack tip, with the mesh defined by radial lines focused on the tip, has shown that the narrow bands of uniform elements near the crack tip in Figure 2 are important for the accuracy.

Examples of plastic zones are illustrated in Figure 2 in terms of dots in deformed meshes, where a dot is drawn at integration points currently undergoing plastic yielding. Figures 2(a) and (b) are obtained for $K_{II}/K_I = -1/2$ under small scale yielding (full details of the models are given in the next section), in one case for the PSB above the crack plane and in the other with the band below. Figure 2c, shows a portion of the mesh and yielded elements for large scale yielding of the full edge-cracked geometry, in this instance for the case where slip can occur wherever the critical shear stress is attained on a slip plane. Concentrated plastic shearing on the extended crack plane and perpendicular to the crack plane emerging from above the tip is clearly seen in Figure 2. The concentrated shearing is accompanied by diffuse plastic shearing, usually in one of the two directions but not the other.

Crack tip displacements (δ_t, δ_n) are sensitive to near tip mesh layout. The opening and sliding displacements behind the tip have a fairly steep variation with distance r back from the tip (Saeedvafa and Rice, 1992), such that the derivative of these quantities with respect to r can be logarithmically singular at the tip. To accurately compute (δ_t, δ_n), it is best to use crack face displacements at points behind the tip and extrapolate to the tip. If $\mathrm{d}\delta/\mathrm{d}r = A - B\ln(r)$, then near the tip,

$$\delta = Ar - B(r\ln r - r) + \delta(0), \tag{2.2}$$

where $\delta(0)$ is the desired value at the tip. One method which has been employed here is to fit (2.2) to sets of values at three points r behind the tip, providing the extrapolation for (δ_t, δ_n).

2.2. Double slip zone models

As evident in Figure 2, much of the plastic deformation occurs by concentrated shearing on the extended crack plane and on the plane perpendicular to it that emerges from the crack tip. If one is willing to neglect the contribution of diffuse plastic deformation in regions off

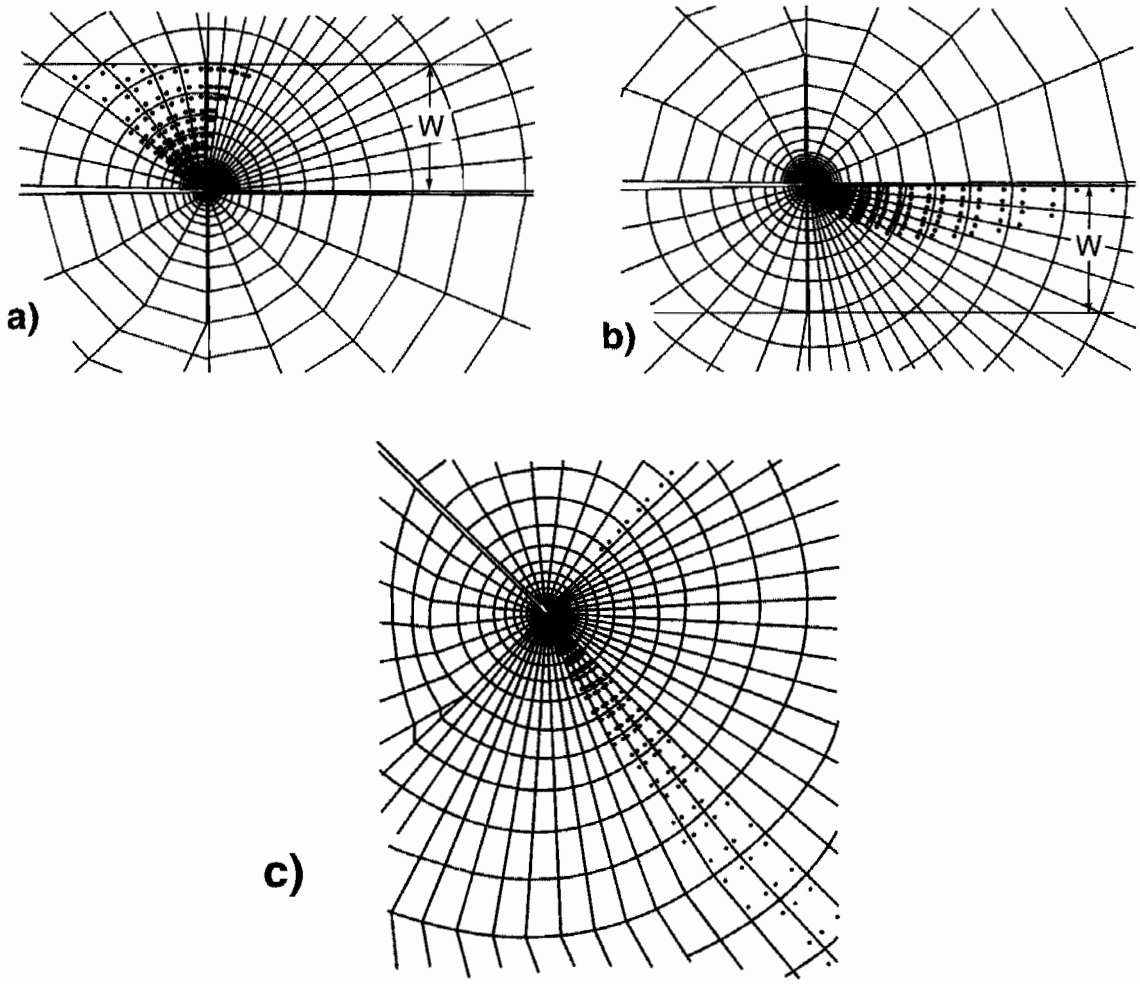

Figure 2. Examples of the near tip finite element mesh and zones of plastic yielding, as indicated by dots at integration points where the yield condition is met. Strips of narrow elements of uniform width are incorporated in the mesh on the extended crack plane and emerging from the tip at 90° to the crack plane. These are required to represent the localized slip along the slip plane and perpendicular to it. Cases (a) and (b) are for small scale yielding with slip confined to a band either above or below the crack plane. Case (c) is an example of large scale yielding where slip is unconfined.

these two planes, one can employ a double slip zone model akin to the Dugdale–Barenblatt Model. In the present plane strain model for the single crystal, the tangential displacement is allowed to be discontinuous across the slip zone when the resolved shear stress attains τ_Y. One advantage of the double slip zone approximation is there exist efficient numerical methods for solving the integral equations for the distributions of the 'dislocations', $d\delta/dr$, that become the unknowns in these formulations. Several such examples are solved in this paper for the purposes of illustrating the approach. Another advantage of these models is that the two crack tip displacements (δ_t, δ_n) are readily expressed and computed in terms of the dislocation distributions. As is standard in such models, the extent of the zone is determined by the condition that the stresses are bounded at the end of the zone, assuming it is not blocked.

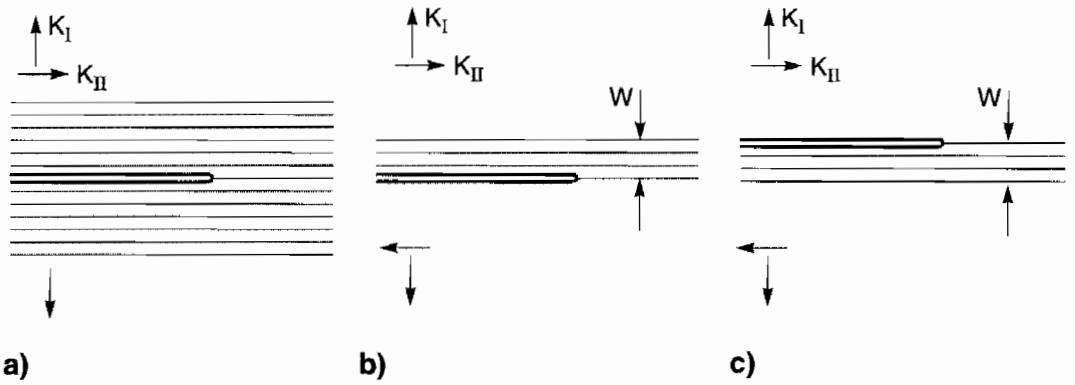

Figure 3. Conventions in small scale yielding. Slip is unconfined in (a), while it is confined to a band of width w above or below the crack plane in (b) and (c). The slip planes are parallel to the crack plane.

3. Small scale yielding

3.1. Pure mode reference cases

Two small scale yielding results will serve as useful references in the present study. In *pure mode II* ($K_I = 0$, with monotonically increasing K_{II} in Figure 3) the analog of the Dugdale–Barenblatt Model applies with slip confined to the single plane coincident with the extended crack plane directly ahead of the tip. The normal component of the crack tip opening displacement, δ_n, is zero and the tangential component, δ_t, is given by

$$\delta_t = (1 - \nu^2)\frac{K_{II}^2}{E\tau_Y}. \tag{3.1}$$

The extent of the plastic slip zone ahead of the tip is $R_t = (\pi/8)(K_{II}/\tau_Y)^2$. If frictional effects between the crack faces are ignored, the amplitude of the change in δ_t in each cycle under a *steady cyclic loading history* with the mode II stress intensity factor varying between K_{II}^{min} and K_{II}^{max} is

$$\Delta\delta_t = \tfrac{1}{2}(1 - \nu^2)\frac{\Delta K_{II}^2}{E\tau_Y}, \tag{3.2}$$

where $\Delta K_{II} = K_{II}^{max} - K_{II}^{min}$.

When the small scale yielding conditions are pure mode I ($K_{II} = 0$ in Figure 3a), the solution for monotonically increasing K_I has been given by Saeedvafa and Rice (1992) for the case where slip on any plane parallel to the crack is possible. The tangential sliding displacement is zero while the opening displacement at the tip is

$$\delta_n \cong 0.26\frac{K_I^2}{E\tau_Y} \quad (\text{for } \nu = 0.3). \tag{3.3}$$

The amplitude of the tip opening displacement under steady cyclic loading between K_I^{min} and K_I^{max} is

$$\Delta\delta_n \cong 0.13\frac{\Delta K_I^2}{E\tau_Y} \quad (\text{for } \nu = 0.3), \tag{3.4}$$

where $\Delta K_{\mathrm{I}} = K_{\mathrm{I}}^{\max} - K_{\mathrm{I}}^{\min}$, assuming no contact occurs between the crack faces.

3.2. Monotonic loading with $K_{\mathrm{II}}/K_{\mathrm{I}} = -1/2$

Under monotonic stressing, the edge-crack in Figure 1 satisfies small scale yielding for applied stresses σ up to approximately one half of the tensile yield stress of the uncracked crystal, i.e. for σ as large as about τ_Y. Under steady cyclic loading, the range of applicability of small scale yielding is considerably larger (i.e., $\Delta\sigma$ as large as about $2\tau_Y$), as will be discussed later. Thus, with reference to Figure 3, consider the small scale yielding limits of the three problems of Figure 1 where a semi-infinite crack is remotely subject to a mixed mode elastic field with amplitudes $(K_{\mathrm{I}}, K_{\mathrm{II}})$. For monotonic loading, the solution will be presented in the form

$$\delta_n = c_n \frac{K_{\mathrm{I}}^2}{E\tau_Y} \quad \text{and} \quad \delta_t = c_t \frac{K_{\mathrm{II}}^2}{E\tau_Y}. \tag{3.5}$$

For the problem in Figure 3(a) where plasticity is not confined to a band, the coefficients (c_t, c_n) are independent of the stress intensities, assuming $K_{\mathrm{II}}/K_{\mathrm{I}}$ is fixed at $-1/2$. A crude estimate of the extent of the plastic zone perpendicular to the crack line is

$$R_n \equiv \frac{1}{9\pi}\left(\frac{K_{\mathrm{I}}}{\tau_Y}\right)^2 \tag{3.6}$$

This quantity serves as a useful scaling length for presenting the solution. For the two PSB problems in Figures 3(b) and 3(c), the coefficients (c_t, c_n) will depend on R_n/w when the plastic zone is large enough such that it reaches across the PSB. Small scale yielding in the present context only requires that the maximum extent of the plastic zone be sufficiently small compared to the crack length. No restriction is placed on its interaction with the boundaries of the PSB.

The coefficients in (3.5) for the problem in Figure 3a where slip is not confined are

$$c_n = 0.35 \quad \text{and} \quad c_t = -0.64. \tag{3.7}$$

Comparison with the pure mode cases in (3.1) and (3.3) reveals that the nonlinear interaction between the modes under mixed mode loading is not exceptionally strong. At comparable stress intensities, the opening displacement is increased by about 20 percent in the presence of the mode II component, while the tangential sliding displacement is lowered by about 30 percent when coupled with the mode I component. Plots of (c_t, c_n) as a function of R_n/w for the two PSB crack problems are shown in Figure 4, together with the values (3.7). (In small scale yielding, the difference between a crack located on one side of the PSB versus the other can be captured by changing the sign of K_{II} without changing the location of the crack relative to the band. However, the PSB results in Figure 4 all have $K_{\mathrm{II}} < 0$ with the crack on top of the band in one case and below it in the other.)

3.3. Cyclic loading with $K_{\mathrm{II}}/K_{\mathrm{I}} = -1/2$

The solution for steady cyclic loading between maximum and minimum stress intensities (with $K_{\mathrm{II}}/K_{\mathrm{I}}$ fixed at $-1/2$) follows immediately from (3.5) for the case in Figure 3(a) where slip is not confined to lie within a band. With $\Delta K_{\mathrm{I}} = K_{\mathrm{I}}^{\max} - K_{\mathrm{I}}^{\min}$ and $\Delta K_{\mathrm{II}} = K_{\mathrm{II}}^{\max} - K_{\mathrm{II}}^{\min}$,

$$\Delta\delta_n = \tfrac{1}{2} c_n \frac{\Delta K_{\mathrm{I}}^2}{E\tau_Y} \quad \text{and} \quad \Delta\delta = \tfrac{1}{2} c_t \frac{\Delta K_{\mathrm{II}}^2}{E\tau_Y}, \tag{3.8}$$

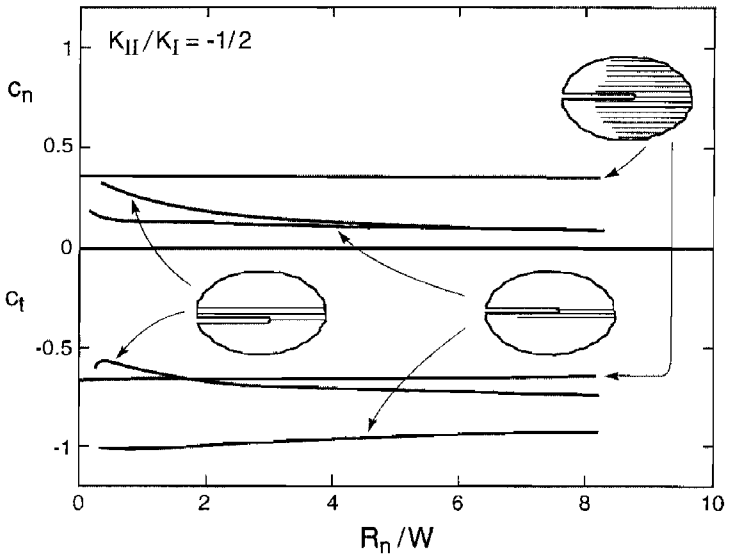

Figure 4. The coefficients specifying the crack tip displacement components in (3.5) for monotonic stressing of the 45° edge-crack under small scale yielding. The length quantity R_n is defined in (3.6), and w is the width of the band of confined slip in two of the three cases shown. In the third case, slip is not confined.

where c_n and c_t have been given (3.7). The argument for the validity of this simple conversion of the monotonic solution to the cyclic solution is essentially the same as that put forward by Rice (1967) in his analysis of Mode III cracks in elastic-perfectly plastic solids. In small scale yielding, the monotonic solution necessarily has the property that once slip starts at any point it continues with the magnitude of the resolved shear stress unchanging at τ_Y. Yielding spreads in a self-similar manner. When the applied stress intensity factors decrease from their maximum values, the *changes* in the stresses, strains and displacements are related to the *changes* in stress intensities precisely by the monotonic solution (with due regard for sign changes) if τ_Y is replaced by $2\tau_Y$. Any point which undergoes reversed yield will have experienced a change in shear stress from $\pm\tau_Y$ to $\mp\tau_Y$, and the superposition of the changes calculated with a yield stress $2\tau_Y$ exactly represents the behavior. The portion of the steady cycle wherein the stress intensities are reversed once more and brought back to their former maximum values is again characterized by changes computed from the monotonic solution with a yield stress of $2\tau_Y$. At the top of the cycle, the stresses and the crack tip displacements return to the values they had before any load reversal occurred.

The shape of the active zone which experiences cyclic plastic strains under steady cyclic loading in small scale yielding is precisely the same as that of the zone under monotonic loading, but the size scales with $(\Delta K/2\tau_Y)^2$ rather than $(K_{\max}/\tau_Y)^2$. It follows that the size of zone of cyclic plastic strains is exactly $(1/4)(\Delta K/K_{\max})^2$ times the size of the monotonic plastic zone at K_{max}. In particular, for cycling between $K_{\max}$ and $K_{\min} = 0$, the cyclic zone is one quarter the size of the monotonic zone, neglecting any possible effects of crack closure. The relatively small size of the cyclic plastic zone has important implications for the relevance of the small scale yielding results. Even when the maximum applied stress drives the monotonic problem well into the large scale yielding range, the cyclic problem may still satisfy small scale yielding. Specifically, cyclic problems for the finite edge-crack geometries posed in Figure 1 remain within the small scale yielding range for cyclic stress amplitudes,

$\Delta\sigma$, less than about $2\tau_Y$. Thus, for example, steady cycling between zero stress and a stress level approaching overall yield at $\sigma = 2\tau_Y$ is still governed by small scale yielding. These considerations highlight the importance of small scale yielding under cyclic loading.

Conversion of the results for monotonic loading to cyclic loading somewhat less straight forward for the PSB cracks because of the dependence on the band width through the parameter R_n/w. Inspection of the numerical solution to the monotonic problem has indicated that it has the property that points which yield undergo no subsequent elastic unloading. This is the necessary condition such that the solution for steady cyclic loading between $K_{\max} - \Delta K$ and $K_{\max}$ can be constructed by the procedure described above using the monotonic solution with τ_Y replaced by $2\tau_Y$. The construction is as follows. Display the dependence of c_n and c_t on R_n/w shown in Figure 4 explicitly by writing $c_n(R_n/w)$ and $c_t(R_n/w)$. Define a quantity for the cyclic problem analogous to R_n in (3.6) as

$$\Delta R_n = \frac{1}{9\pi}\left(\frac{\Delta K_{\mathrm{I}}}{2\tau_Y}\right)^2. \tag{3.9}$$

Then, the cyclic crack tip displacements are given by

$$\Delta\delta_n = \tfrac{1}{2}c_n(\Delta R_n/w)\frac{\Delta K_{\mathrm{I}}^2}{E\tau_Y} \quad \text{and} \quad \Delta\delta_t = \tfrac{1}{2}c_t(\Delta R_n/w)\frac{\Delta K_{\mathrm{II}}^2}{E\tau_Y}, \tag{3.10}$$

where, as before, attention is limited to $\Delta K_{\mathrm{II}} = -\Delta K_{\mathrm{I}}/2$. The condition that no elastic unloading occurs in solution for monotonic loading ensures that the superposition employed in constructing the cyclic solution is valid. For single slip plasticity there are no additional complexities associated with nonproportional plastic deformation.

It can be seen from the plots in Figure 4 that the dependence of c_n and c_t on $\Delta R_n/w$ is quite weak for $\Delta R_n/w$ greater than about 2. For $\Delta R_n/w$ less than 2, the dependence can become important. For example, in the case where the PSB lies above the crack, the fact that c_n decreases with increasing $\Delta R_n/w$ while c_t increases in magnitude means that there is a range where $\Delta\delta_n$ becomes larger than $\Delta\delta_t$.

4. Edge-crack in large scale yielding

The three 45° edge-crack problems in Figure 1 are now considered for monotonically increasing σ. The results are presented as the stress dependent coefficients C_n and C_t in

$$\delta_n = C_n\left(\frac{\sigma}{2\tau_Y}\right)\frac{\sigma^2 a}{E\tau_Y} \quad \text{and} \quad \delta_t = C_t\left(\frac{\sigma}{2\tau_Y}\right)\frac{\sigma^2 a}{E\tau_Y}. \tag{4.1}$$

For the two PSB problems the coefficients also depend on w/a. Within the small scale yielding range, coinciding approximately with $\sigma/(2\tau_Y) < 1/2$, the two sets of coefficients in (3.5) and (4.1) are related by

$$C_n = 1.561c_n \quad \text{and} \quad C_t = 0.416c_t. \tag{4.2}$$

The coefficients are plotted in Figure 5. The small scale yielding limit as given by (4.2) with (3.7) is included in Figure 5(a) for the problem with no restrictions on the zone of plastic yielding ($C_n = 0.55$ and $C_t = -0.27$). Both components of the crack tip displacement

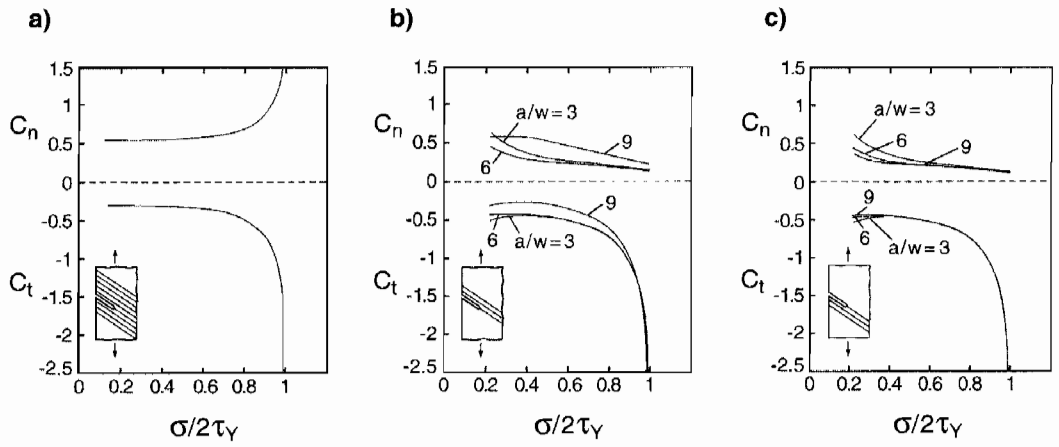

Figure 5. The coefficients specifying the crack tip displacement components in (4.1) for monotonic stressing of the 45° edge-crack under large scale yielding. (a) Unconfined slip. (b) Slip confined to a band of width w above the crack plane. (c) Slip confined to a band of width w below the crack plane.

experience large amplification due to large scale yielding, in the range $\sigma/(2\tau_Y) > 1/2$. The PSB problems display some dependence on a/w, but surprisingly little over the range of values of a/w chosen in Figure 5. The tangential component of the tip displacement follows the behavior of the problem with unconstrained yield. On the other hand, the band severely constrains the magnitude of the opening component in the large scale yielding range compared to the case where slip is not confined. An unexpected trend is noted in Figure 5(b) for the case where the PSB lies on the upper side of the crack. The normal component of the crack tip displacement is larger for the narrowest band ($a/w = 9$) than for the wider bands ($a/w = 6$ and 3). This trend is a consequence of the nonlinear coupling between the opening and tangential tip displacements under the mixed mode loading. Note that the tangential component is diminished by the narrowness of the band. These same trends can be inferred from the small scale yielding results in Figure 4, although they are obscured by the nondimensional variables used in that figure.

The double slip zone model discussed in Section 2.2 can be used to approximate the problems in Figures 1 and 3. As mentioned in Section 2.2, well established numerical methods for integral equations can be employed to generate results, and crack tip displacement components are readily extracted. A set of results for C_n and C_t in (4.1) for the two PSB problems is given in Figure 6. Included is the result for δ_t for the limit of a band of zero width ($w/a = 0$ such that $\delta_n = 0$), and results for bands of small width, $w/a = 0.05$, located on one side of the crack or the other. These numerical results are in reasonable agreement with the finite element results for the unapproximated model, and the general trends are in close accord.

As has already been emphasized, the responses under steady cyclic loading should be well characterized by the small scale yielding results given in the previous section, assuming that $\Delta\sigma$ is less that about $2\tau_Y$.

5. Barriers to slip

To obtain some insight into the effect of barriers to slip such as a grain boundary, two variations of the 45° edge-crack problem have been analyzed. The first imposes a boundary a distance D along the crack plane from the edge, across which slip is completely blocked.

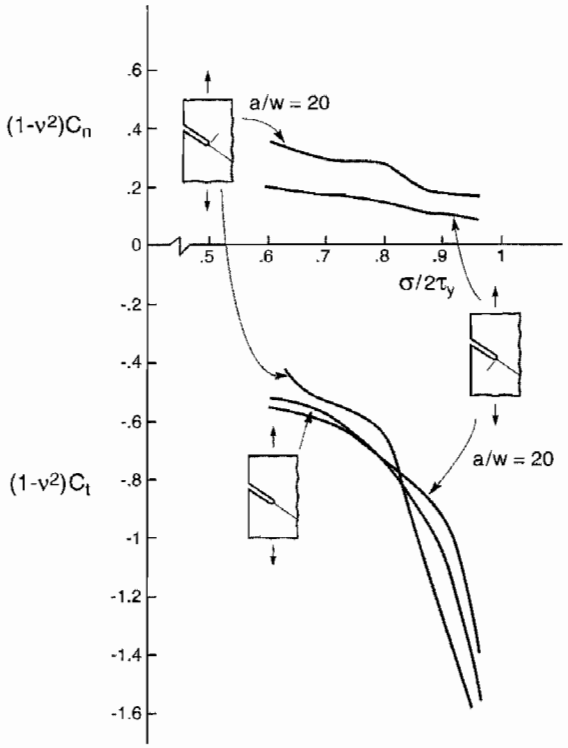

Figure 6. The coefficients specifying the crack tip displacement components in (4.1) for monotonic stressing of the 45° edge-crack under large scale yielding as computed using the double slip zone model of Section 2.2. Three cases are shown: a single slip zone on the extended crack plane for which $C_n = 0$, and double slip zones with $a/w = 20$ modeling bands above and below the crack plane.

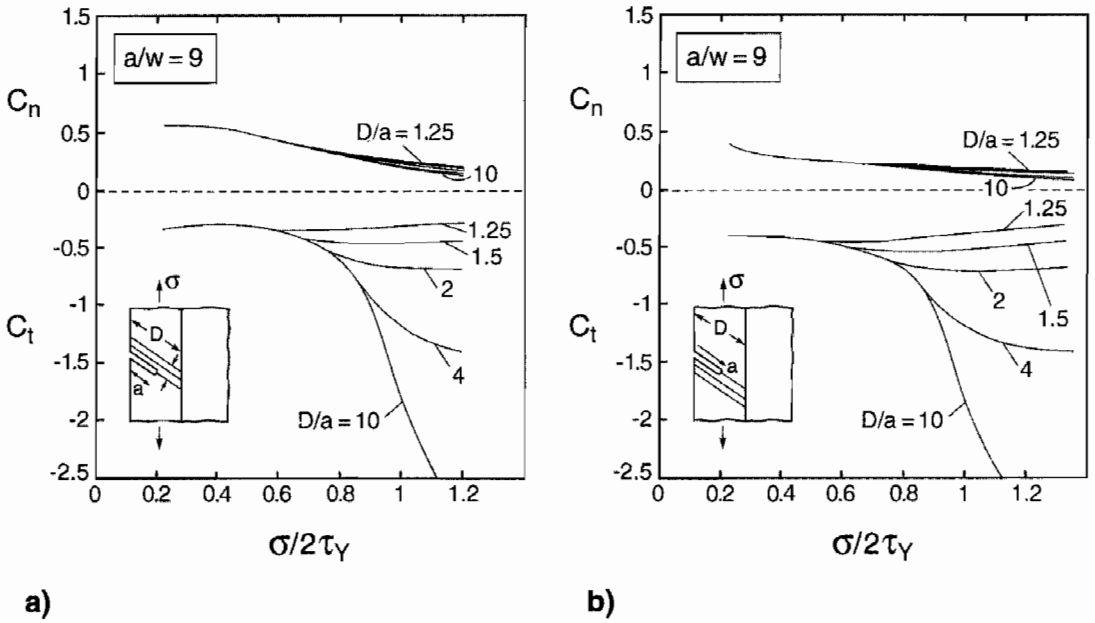

a) **b)**

Figure 7. The coefficients specifying the crack tip displacement components in (4.1) for monotonic stressing of the 45° edge-crack under large scale yielding where slip is blocked a distance D from the edge in the slip direction. Slip confined to a band of width w above the crack in (a) and below the crack in (b), in both cases with $a/w = 9$.

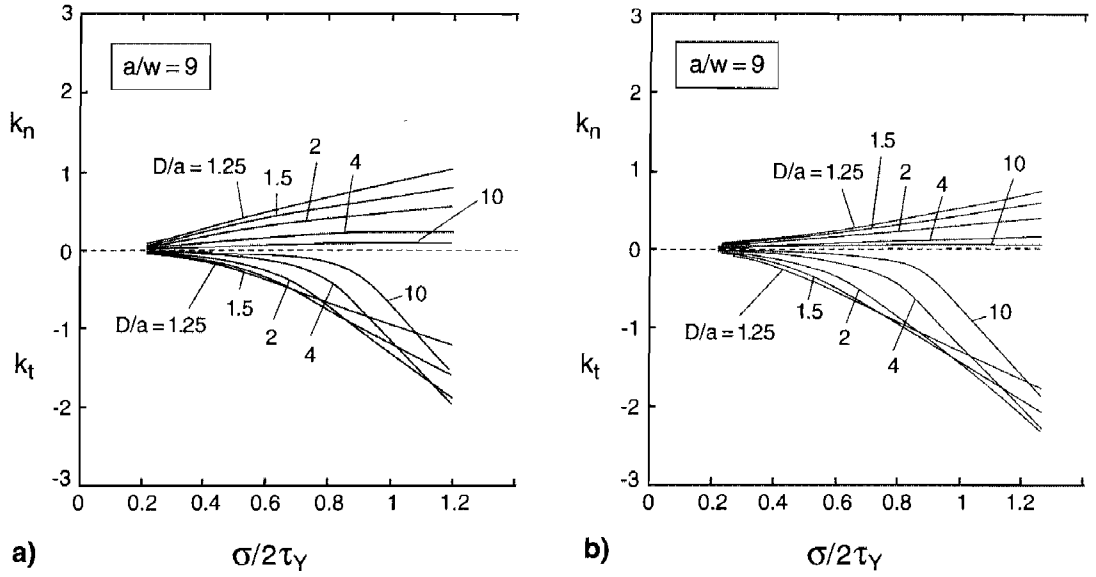

Figure 8. The coefficients specifying the crack tip displacement components in (5.1) for monotonic stressing of the 45° edge-crack under large scale yielding where slip is blocked a distance D from the edge in the slip direction. Slip confined to a band of width w above the crack in (a) and below the crack in (b), in both cases with $a/w = 9$. These are the same results shown in Figure 7, but here another normalization is employed to better reveal the influence of crack length at different positions of the crack relative to the slip barrier.

Only elastic deformations occur across the boundary. The second variation permits slip across the boundary, activated by the same critical shear stress τ_Y, but on a plane oriented at an angle ω relative to the slip plane in the cracked crystal. In both instances, monotonic loading is considered, but the effects are expected to carry over to cyclically loaded cracks as they approach slip barriers and their plastic zones are restricted.

5.1. Blocked slip

Plots of C_n and C_t as defined in (4.1) are given in Figure 7 for five values of D/a. The values for the largest value, $D/a = 10$, essentially coincide with the limiting case $D/a = \infty$ presented earlier in Figure 5. For values of $\sigma/(2\tau_Y)$ less than 1/2, there is no effect of the barrier even when $D/a = 1.25$ because the plastic zone has not yet reached the boundary. For larger applied stresses, the plastic zone is blocked by the boundary, depending on D/a, and the tangential component of the tip displacement, δ_t, becomes substantially reduced. The opening tip displacement is much less affected. The magnitude of the opening displacement becomes comparable to the tangential component when D/a is about 1.25.

The normalization (4.1) used for the tip displacements in Figure 7 is not convenient for seeing the influence of the boundary on an approaching crack. This same set of numerical data is replotted in Figure 8 using the following normalization which employs the boundary distance in the normalization rather than the crack length:

$$\delta_n = k_n \frac{\tau_Y D}{E} \quad \text{and} \quad \delta_y = k_t \frac{\tau_Y D}{E}. \tag{4.2}$$

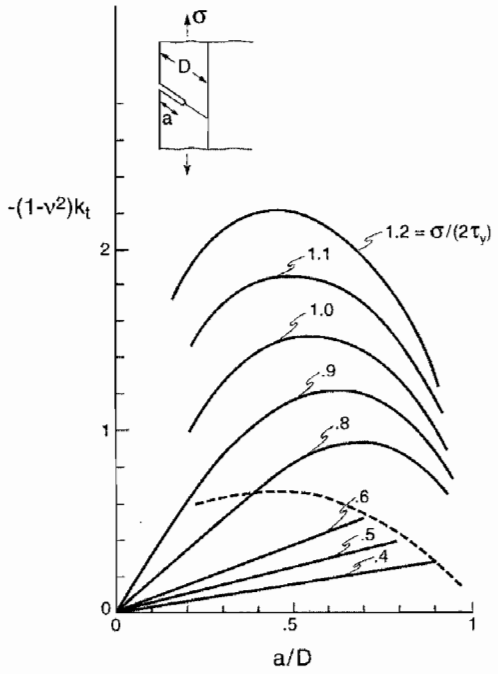

Figure 9. The coefficient k_t in (5.1) governing the tangential tip displacement as predicted by a single slip zone model with slip confined to the plane ahead of the crack tip. Slip is blocked a distance D along the plane from the edge. The straight line segments emanating from the origin correspond to the region where the slip zone has not yet reached the barrier.

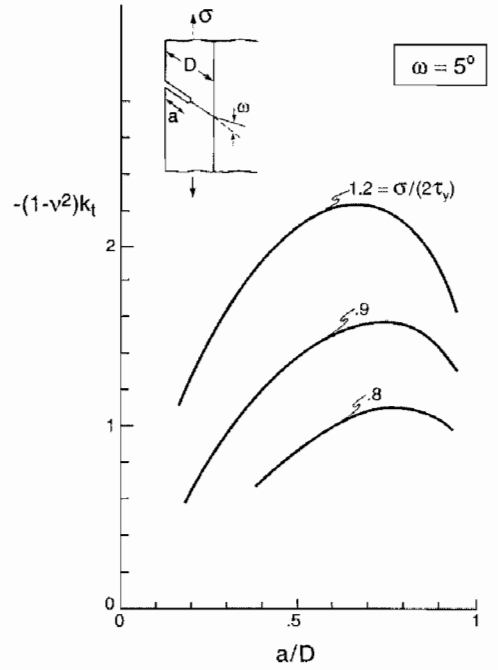

Figure 10. The coefficient k_t in (5.1) governing the tangential tip displacement as predicted by a single slip zone model with slip confined to the plane ahead of the crack tip. Slip is partially blocked a distance D along the plane from the edge. Beyond this boundary, the orientation of the slip plane changes. The results were obtained with a model which permits slip only on the single planes shown in the insert.

In this plot is evident that the crack tip displacements are larger as the crack travels across the crystal at a given applied stress, but the boundary holds down the magnitudes at the higher applied stress levels. In particular, the tangential tip displacement component peaks at a value of D/a below 1.25 at the higher applied stress levels. Predictions for k_t for the tangential component of the tip displacement from a single slip zone model with slip blocked at the boundary are plotted in Figure 9 against a/D. The straight line segments of the curves emanating from the origin within the dashed-line curve correspond to the regime where the yielding zone has not reached the boundary. Beyond the dashed-line curve, the boundary interferes with slip, and the crack tip displacement is significantly reduced.

5.2. Partially blocked slip

The model of Figure 9 is modified by allowing slip to occur across the boundary, but on a slip system oriented at an angle other than 45°. The model depicted in Figure 10 permits slip at a critical stress τ_Y, consistent with (1.3), on a single plane intersecting the primary 45° slip plane at an angle ω. The results in Figure 10 have been obtained for a small misorientation of the slip planes, $\omega = 5°$. Comparison of Figures 9 and 10, reveals that slip across the boundary does have some influence on the tangential tip displacement, but even with a small misorientation of the slip direction, the boundary serves as an effective block to the slip zone of the edge crack.

6. Concluding remarks

The small scale yielding solution describes cyclic crack tip behavior under steady cycling for a fairly wide range of stress because the cyclic plastic zone size is a small fraction of the monotonic zone size. Under the assumption that small scale yielding does apply, the 45° edge-crack subject to steady cyclic stressing between $\sigma_{\min}$ and $\sigma_{\max}$ experiences cyclic tip displacements which can be obtained from (1.1), (3.1) and (3.3) (by replacing τ_Y by $2\tau_Y$ as discussed in Section 3.3) as

$$\Delta\delta_n = 0.275\frac{\Delta\sigma^2 a}{E\tau_Y} \quad \text{and} \quad \Delta\delta_t = 0.135\frac{\Delta\sigma^2 a}{E\tau_Y}, \tag{6.1}$$

where $\Delta\sigma = \sigma_{\max} - \sigma_{\min}$. This result applies to the case where slip in the crystal is unconfined, and there is no crack face contact. When an obstacle or grain boundary is sufficiently close to the crack tip such that it interacts with the cyclic plastic zone, that interaction must be taken into account. The solutions in the present paper provide some insight into such interactions, but further studies will be needed to provide results which are applicable under cyclic loadings. Most Stage I fatigue cracks appear to be arrested by obstacles or barriers (Miller, 1993), and quantitative results for these interactions are needed to understand condition under which arrest occurs.

Attention here has been limited to applied stress levels such that the crystal itself does not experience overall yielding. In the range of cyclic stressing causing fatigue in a polycrystal, a small fraction of surface crystals favorably oriented for slip are expected to experience overall reversed plastic straining in each cycle. Were this not the case, it is unlikely fatigue crack nucleation would occur. Thus, an important extension of the present study will be to consider Stage I edge cracks lodged within favorably oriented crystals which experience reversed plastic straining each cycle even when no crack is present.

Components of the crack tip displacements have been featured in this study under the assumption that these quantities provide average measures of crack tip deformation which should provide a means of correlating crack growth rates. Further experimentation and more fundamental modeling are needed to relate crack growth per cycle to the amplitudes of the crack tip displacements under Stage I, when cracks tend to grow along the favorably oriented slip directions. In particular, the effect on the growth rate of the ratio of the normal to tangential tip displacements must be determined since the relative amplitude appears to vary considerably, depending on the cyclic stress level and on proximity to obstacles to slip.

Acknowledgment

The work of J.W.H. was supported in part by the MURI on High Cycle Fatigue from AFOSR and in part by the Division of Engineering and Applied Sciences, Harvard University. The work of V.T. is partly supported by the MUP2 Center for Materials Processing, Properties and Modelling, financed by the Danish Agency for Development of Trade and Industry, the Danish natural Science Research Council, and the Danish Technical Research Council.

References

Barenblatt, G.I. (1959a). The formulation of equilibrium cracks during brittle fracture. General ideas and hypotheses. Axially-symmetric cracks. *Journal of Applied Mathematics and Mechanics* **23**, 622–636. (Translation from Russian: PMM **23** (1959a), 434–444).

Barenblatt, G.I. (1959b). The formulation of equilibrium cracks during brittle fracture. Rectilinear cracks in plane plates. *Journal of Applied Mathematics and Mechanics* **23**, 1009–1029. (Translation from Russian: PMM **23** (1959b), 706–721).

Barenblatt, G.I. (1962). The mathematical theory of equilibrium cracks in brittle fracture. *Advances in Applied Mechanics* **7**, 55–129.

Dugdale, D.S. (1960). Yielding of steel sheets containing slits. *Journal of the Mechanics and Physics of Solids* **8**, 100–108.

Isida, M. (1979). Tension of a half plane containing array cracks, branched cracks and cracks emanating from sharp notches. *Transaction of the Japan Society for Mechanical Engineers* **45**, 306–317.

Ma, B.-T. and Laird, C. (1989). Overview of fatigue behavior in copper single crystals: I, II & III. *Acta Metallurgica* **37**, 325–336, 337–348, 349–355.

McDowell, D.L. (1996). Basic issues in the mechanics of high cycle metal fatigue. *International Journal of Fracture* **80**, 103–145.

Miller, K.J. (1993). Materials science perspective of metal fatigue resistance. *Materials Science and Technology* **9**, 453–462.

Repetto, E.A. and Ortiz, M. (1977). A micromechanical model of fatigue crack nucleation in FCC metals. *Acta Materialia* **45**, 2577–2595.

Rice, J.R. (1967). *Mechanics of Crack Tip Deformation and Extension by Fatigue*. ASTM STP 415, American Society of Testing Materials, 247–309.

Saeedvafa, M. and Rice, J.R. (1992). Crack tip fileds in a material with three independent slip systems: NiAl single crystal. *Modelling and Simulation in Materials Science and Engineering* **1**, 53–71.